AIMS Materials Science, 3(2): 434-447.
DOI: 10.3934/matersci.2016.2.434
Received: 15 February 2016
Accepted: 20 March 2016
Published: 24 March 2016

http://www.aimspress.com/journal/Materials

Research article

Tubular micro- and nanostructures of TCO materials grown by a vapor-solid method

Miguel García-Tecedor [1], Félix del Prado [1], Carlos Bueno [2], G. Cristian Vásquez [1], Javier Bartolomé [1], David Maestre [1,*], Tomás Díaz [2], Ana Cremades [1], and Javier Piqueras [1]

[1] Dpto. Física de Materiales, Facultad de CC. Físicas, Universidad Complutense de Madrid, 28040, Madrid, Spain
[2] Centro de Investigación en Dispositivos Semiconductores, Benemérita Universidad Autónoma de Puebla (BUAP), Puebla, México

* **Correspondence:** Email: dmaestre@ucm.es.

Abstract: Microtubes and rods with nanopipes of transparent conductive oxides (TCO), such as SnO_2, TiO_2, ZnO and In_2O_3, have been fabricated following a vapor-solid method which avoids the use of catalyst or templates. The morphology of the as-grown tubular structures varies as a function of the precursor powder and the parameters employed during the thermal treatments carried out under a controlled argon flow. These materials have been also doped with different elements of technological interest (Cr, Er, Li, Zn, Sn). Energy Dispersive X-ray Spectroscopy (EDS) measurements show that the concentration of the dopants achieved by the vapor-solid method ranges from 0.5 to 3 at.%. Luminescence of the tubes has been analyzed, with special attention paid to the influence of the dopants on their optical properties. In this work, we summarize and discuss some of the processes involved not only in the anisotropic growth of these hollow micro and nanostructures, but also in their doping.

Keywords: microtube; nanopipe; transparent conductive oxide; cathodoluminescence

1. Introduction

Most of the recent advances in nanoscience and nanotechnology are based on the relevant achievements reached in the synthesis of materials with desirable dimensions, morphology and composition, as well as in their subsequent use as building blocks in many fields of technological

research. In this way, a precise control of the synthesis process is required in order to exploit the capabilities of low dimensional materials, for which many synthesis approaches have been followed so far. Among the most challenging and promising morphologies, tubular micro- and nanostructures are attracting increasing attention due to their characteristic geometry which confers them improved performances. In particular, apart from the widely investigated carbon nanotubes [1], some other tubular micro and nanostructures of different materials are facing challenging performance in energy storage, environmental applications, sensing and optoelectronics [2,3,4]. Despite the growing interest on the applicability of tubular structures, their fabrication is not an easy task and several synthesis methods are being employed, as for instance electrospinning, hydrothermal, or template-based methods [5,6,7], being the latter the most commonly used. However, the tubes synthesized by these procedures are usually polycrystalline and mesoporous, instead of highly crystalline materials. In order to optimize the fabrication of these characteristic hollow structures, their growth mechanisms in different materials still require to be further understood and controlled.

In this work we report on the synthesis of micro and nanotubes of different transparent conductive oxides (TCO), such as SnO_2, TiO_2, ZnO and In_2O_3, by a vapor-solid (VS) method which avoids the use of catalyst or templates [8,9,10]. Some other growth methods, such as vapor-liquid-solid (VLS) [11], or solid-liquid-solid (SLS) [12] require the use of a catalyst, usually Au, in form of drops or a thin film, which governs the anisotropic growth of elongated nanostructures achieving ordered arrays of the nanostructures on a substrate. However, the presence of the catalyst in the as-grown structures is hardly avoided, and usually nanowires decorated with Au or with Au at the tip are obtained by these methods, which could be detrimental for some applications. Besides, usually wires, but not tubes, are grown by VLS and SLS methods. The VS method avoids the use of catalysts and leads to the growth of structures with a wide variety of morphologies, including tubes, which confers higher versatility to this method. On the other hand, contrary to the VLS method, a wide dispersion of sizes is usually obtained by the VS method as the control of the dimensions of the as grown micro- and nanostructures is not easy in this case. The VS method employed in this work results in large concentrations of high crystalline quality materials in form of tubes and also in other forms such as wires, arrows, rods, or complex structures. In particular, the tubes are good candidates to be used in optoelectronics, as well as in sensors and bio-chemical molecular detection and environmental applications, as recently reported by different authors [13,14,15]. As an example, the optical response of ZnO microtubes can be modulated when filled with a fluid [16]. Moreover, Sn filled ZnO nanorods have been recently proposed to be used as thermal nanosensors, soldering and electrical nanocomponents [17], whereas ZnO microtubes have shown good properties as optical resonators [18].

In this work also the doping of the tubes with different elements of technological interest, such as Cr, Er, or Li in the case of SnO_2 microtubes, Cr for TiO_2, and Zn or Sn for the In_2O_3 samples, has been investigated. Energy Dispersive X-ray spectroscopy (EDS) has been used to study and quantify the presence of dopants in the samples. The effects caused by doping on the optical properties of the tubes are analyzed by cathodoluminescence (CL). Mechanisms involved in the formation of the tubes, such as screw-dislocation driven growth, are also discussed.

2. Materials and Method

The synthesis method employed by our group for the growth of the tubes is based in a catalysis-free vapor-solid process [8]. The precursor powder is pressed into pellets and placed in a

furnace. Afterwards, thermal treatments are carried out under a controlled argon flow at different temperatures (600–1400 ºC) as a function of the precursor. For the growth of the doped tubes, the initial powder is mixed with a dopant-based material in a controlled weight ratio. In this work, undoped SnO_2 microtubes have been grown using SnO_2 powder as precursor, while Cr, Er or Li doped SnO_2 microtubes have been fabricated by using an initial mixture of SnO_2 and Cr_2O_3 (5% wt.), Er_2O_3 (5% wt.) or Li_2CO_3 (5% wt.), respectively. Cr doped rutile TiO_2 microtubes have been fabricated using either TiN mixed with Cr_2O_3 (10% wt.) or Cr doped TiO_2 nanoparticles (Cr 10% cat.) as precursors. ZnO tubes have been grown using metallic Zn as initial powder. In the case of In_2O_3, rods with nanopipes in the core were synthesized using either InN or In_2S_3 as precursors. Sn or Zn doped In_2O_3 rods and microstructures showing pipes have been fabricated by adding SnO_2 (10% wt.) or ZnO (5% wt.), respectively to the initial powders.

The micro and nanotubes were characterized by using different techniques. X-ray Diffraction (XRD) measurements were performed in a Philips X'Pert Pro diffractometer using Cu K_α radiation. In the study of the morphology, a Leica 440 Steroscan and a Fei Inspect Scanning Electron Microscopes (SEM) were used. Transmission Electron Microscopy (TEM) characterization was carried out using a Philips CM30 TEM operated at 300 kV. Cathodoluminescence (CL) spectra were acquired in a Hitachi S2500 SEM using a Hamamatsu PMA-11 charge-coupled device camera. A Bruker AXS Quantax system was used for the Energy Dispersive X-Ray Spectroscopy (EDS) measurements and a Bruker e-FlashHR+ electron backscattered diffraction (EBSD) system was employed for the structural analysis of the microtubes.

3. Results and Discussion

3.1. Rutile microtubes (SnO_2, TiO_2)

Figure 1a shows a SEM image where a high amount of SnO_2 microtubes, grown by thermal treatments at 1400 ºC during 10 hours, can be observed. These tubes have been grown on the surface of the pellet, which in this case acts as source of material and substrate, and they show lengths up to hundreds of microns and widths between a few and tens of microns. These tubes, with widths ranging from hundreds of nm to few microns, show square or rectangular sections [8]. The microtubes can be easily detached from the surface of the pellet and manipulated in order to complete their study and to be used as building blocks in optoelectronic devices. XRD and EBSD measurements, not shown here, show that the lateral faces of the tubes correspond to the {110} planes of rutile SnO_2 and that the tubes grow along the [001] direction, as schemed in the inset of Figure 1a. By modifying the composition of the initial powders, doped SnO_2 tubes can be also achieved. As an example, Cr doped SnO_2 microtubes are fabricated at 1400 ºC by mixing SnO_2 and Cr_2O_3 (5% wt.) in the precursor powder. The dimensions of the tubes are similar to the undoped ones, but in this case the lateral faces are smoother and thinner, and occasionally tubes with peaked endings are observed, as shown in Figure 1b. These tubes exhibit new optical properties as compared with the undoped ones. In particular, the Cr doped SnO_2 tubes are purplish, as observed in the optical image in the inset of Figure 1b, while the undoped SnO_2 microtubes are transparent in the visible range. If Er_2O_3 (5%wt.) is added to the initial mixture, Er doped SnO_2 microtubes can be grown at 1400 ºC [19], as shown in Figure 1c. In this case the surfaces of the tubes are more irregular, as shown in the inset of Figure 1c, and appear usually with cracks. In addition, the resistivity of these tubes increases due to the Er doping, as denoted by charge effects during SEM

observation. Also Li doped SnO_2 microtubes have been fabricated at 1400 ºC by adding Li_2CO_3 (5% wt.) in the initial powders, as shown in Figure 1d. In that case, the tubes show a smoother appearance and higher dimensions, as compared with undoped ones. However, in some cases, the Li doped tubes exhibit a high irregular ending formed by complicated microstructures, as observed in the inset of Figure 1d. The doped tubes also grow along the [001] direction and are formed by {110} surfaces, as demonstrated by XRD and EBSD measurements (not shown here). These surfaces are reported to be the more stable for rutile materials such as SnO_2 and TiO_2 [20,21]. Beltran et al. [22] calculated the stability conditions and energetic cost of the different SnO_2 stoichiometric surfaces. Their calculations indicate that the (110) surface is the most stable which is in agreement with the results obtained by EBSD of the rutile tubes. The (001) and (201) planes have a relative higher surface energy, which may lead to a growth along these directions in agreement with the [001] assignment for the growth direction of the rutile tubes, based on Raman polarized measurements.

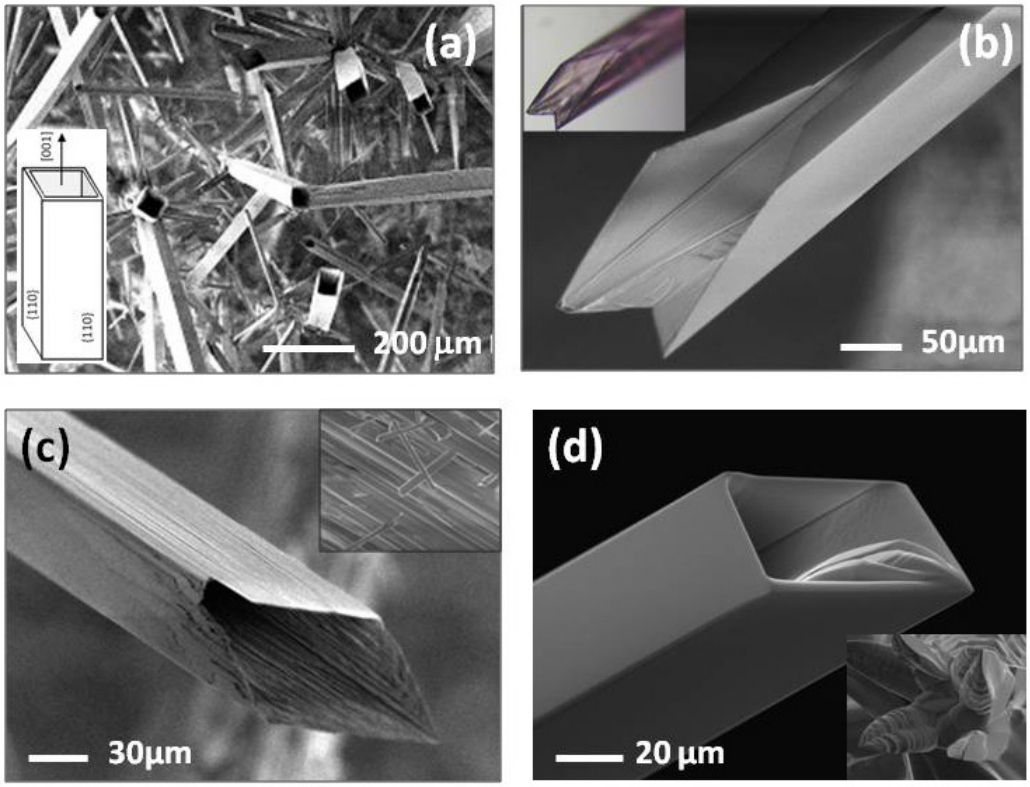

Figure 1. SEM images of (a) undoped SnO_2 microtubes, (b) Cr doped, (c) Er doped and (d) Li doped microtubes. The corresponding insets show (a) a scheme of the tubes, (b) an optimal image of the Cr doped SnO_2 tubes, (c) a detail of the surface of the Er doped SnO_2 tubes, and (d) a detail of some of the complex structures appearing at the apex of the Li doped SnO_2 tubes.

In order to investigate the effects of the dopants on the optical properties of the SnO_2 tubes, CL of the undoped and doped tubes has been investigated. Figure 2 shows the CL spectra of the undoped and the Cr and Li doped SnO_2 microtubes. The presence of dopants clearly modifies the luminescence of the tubes, as observed in the CL spectra shown in Figure 2, acquired at 18 kV and room temperature.

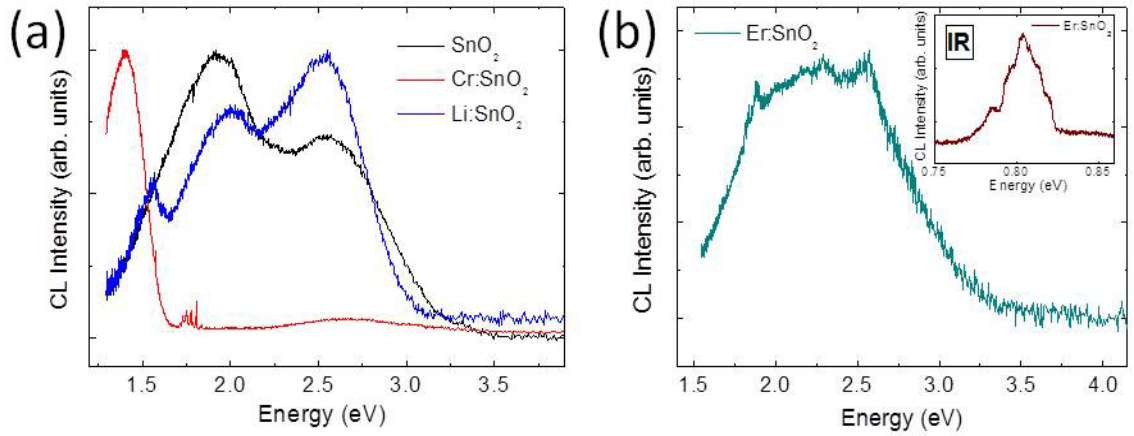

Figure 2. (a) CL spectra of undoped SnO_2 microtubes and Cr doped and Li doped SnO_2 microtubes. (b) CL spectrum acquired on Er doped SnO_2 microtubes. The corresponding CL spectrum in the IR range is shown in the inset.

The wide bandgap of SnO_2 (3.6 eV) provides luminescence in a wide spectral range. In particular, CL emission from undoped SnO_2 mainly consists of three emissions centered around 1.94 eV, 2.25 eV and 2.58 eV, known as orange, green and blue bands respectively [23]. The orange band is associated with oxygen vacancies related defects and, although the origin of the green band is still under discussion, most works also associate this emission with oxygen deficiency [8,24,25]. The blue band is usually related to transitions involving surface defects. The presence of dopants alters the concentration of these defects, which modifies the CL signal. Moreover, new emissions associated with the dopants can be also generated. Cr doping drastically alters the luminescence of SnO_2 (Figure 2a). The characteristic visible emission of SnO_2 is quenched due to the Cr doping and a new emission around 1.4 eV dominates the corresponding CL spectrum, as shown in Figure 2a. Narrow emission lines can be also observed at 1.8 eV which are related to Cr^{3+} intraionic transitions [26]. Doping with Li also modifies the luminescence of SnO_2, but in this case the CL spectrum is more similar to the undoped SnO_2. Apart from the orange, green and blue bands, the relative intensities of which change with respect to undoped SnO_2, a new emission appears at around 1.6 eV, which is associated with the Li doping. When doping with Er, in addition to the characteristic emissions of SnO_2, narrow weak emissions appear at 1.87 eV and 2.23 eV. These emissions are associated with Er^{3+} 4f intraionic transitions [19], in particular to $^4F_{9/2}$ -$^4I_{15/2}$ (1.87 eV) and $^4S_{3/2}$-$^4I_{5/2}$ (2.23 eV). Moreover, an infrared emission at 0.8 eV appears (Figure 2b), related to $^4I_{3/2}$-$^4I1_{5/2}$ Er^{3+} intraionic transitions due to Er^{3+} substituting Sn^{4+} in the SnO_2 lattice [19]. Some of these emissions allow to extend the applicability of SnO_2 in optoelectronic devices. As an example the 0.8 eV emission related to Er doping lies at the region of minimum losses for silica-based waveguides, mainly used in optical communications. The vapor solid method used for the growth of the tubes allows homogeneous doping and low doping content ranging from 0.5–3 at.%, as measured by EDS.

Cr doped TiO_2 microtubes have been also fabricated by the vapor-solid method at 1250–1300 ºC either using Cr doped TiO_2 nanoparticles, or TiN mixed with Cr_2O_3 as initial powders (5–10% cat. Cr) [9]. The tubes show rectangular or squared sections, as the SnO_2 tubes, but in this case the dimensions are lower, of about 5 μm lateral size and tens of micrometers length, as shown in Figures 3a and 3b, corresponding to SEM images of Cr doped microtubes grown from $Ti_{0.9}Cr_{0.1}O_2$

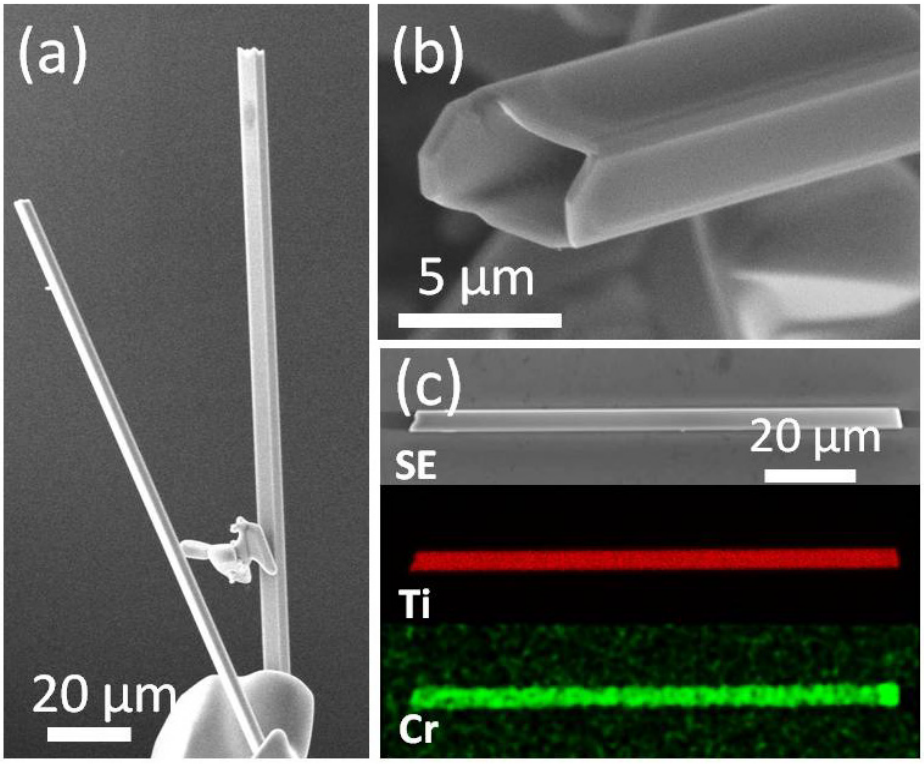

Figure 3. SEM images of Cr doped TiO_2 microtubes grown using (a) $Ti_{0.9}Cr_{0.1}O_2$ nanoparticles or (b) TiN mixed with Cr_2O_3 (10% wt.) powders as precursors. (c) SEM image of a microtube and the corresponding EDS compositional mappings of Ti and Cr.

nanoparticles and TiN mixed with 10% wt. Cr_2O_3, respectively. The maximum Cr content observed in the microtubes by EDS analysis is 3% cationic fraction. The Cr is homogeneously distributed along the microtubes, as observed in the EDS elemental mapping for Ti and Cr shown in Figure 3c. The Chromium concentration can be controlled by the amount of Cr in the precursor powders, as well as by the temperature and duration of the thermal treatments. Combined Raman-EBSD measurements [9] show that the rutile TiO_2 tubes grow along the [001] direction and the lateral faces are formed by {110} surfaces independently of the precursor, in agreement with the results on SnO_2 microtubes. The morphological and crystallographic similarities observed between SnO_2 and TiO_2 microtubes could be due to similar growth mechanisms, since both materials shares the rutile crystalline structure. However, contrary to SnO_2, for which undoped microtubes can be also grown, in the case of rutile TiO_2 the presence of Cr clearly benefits the growth of microtubes which rarely appears for undoped TiO_2. The CL study reveals changes in the luminescent response of the tubes as a function of the final morphology and the employed precursor. Figure 4a shows the normalized CL spectra acquired at room temperature (300 K) from microtubes grown using Cr doped TiO_2 nanoparticles (10% cat.) and TiN mixed with 10% wt. Cr_2O_3. CL spectrum of undoped TiO_2 has been also included as a reference. The characteristic CL spectrum of undoped rutile TiO_2 is dominated by a relatively intense IR band located at 1.52 eV, which is frequently attributed to radiative recombinations related to reduced Ti^{3+} ions induced by oxygen deficiency at the TiO_2 surface [9,27], and a broad and weaker band extended from the visible (VIS) to UV region centered at approximately 2.5 eV, attributed to shallow traps related to oxygen vacancies and other oxygen related defects as *F*-centers or adsorbed oxygen [9]. For the

microtubes grown from the mixture of TiN and Cr_2O_3 powders the IR band is slightly red-shifted but still dominates the CL spectrum, whereas the VIS-UV region shows a decreased relative intensity. In addition, a small narrow band appear at 1.8 eV (marked with an arrow in Figure 4a) associated with intraionic ^2E-^4A transition in Cr^{3+} in octahedral coordination [26], which confirms the incorporation of Cr within the rutile lattice. The opposite behavior can be observed for microtubes grown from Cr doped TiO_2 nanoparticles, as shown in Figure 4a. In that case, the relative intensity of the IR band decreases with respect to the VIS-UV band, which dominates the CL spectrum. Moreover, the VIS-UV band is centered at about 3 eV, which can be due to an increase of near band-edge defects induced by Cr ions. In this case the band at 1.8 eV is not well defined and appears as a weak band. However, reducing the thermal broadening and phonon contribution, by decreasing the temperature down to 100 K (Figure 4b), this band is well defined at 1.8 eV, confirming the presence of Cr^{3+} ions in the rutile lattice.

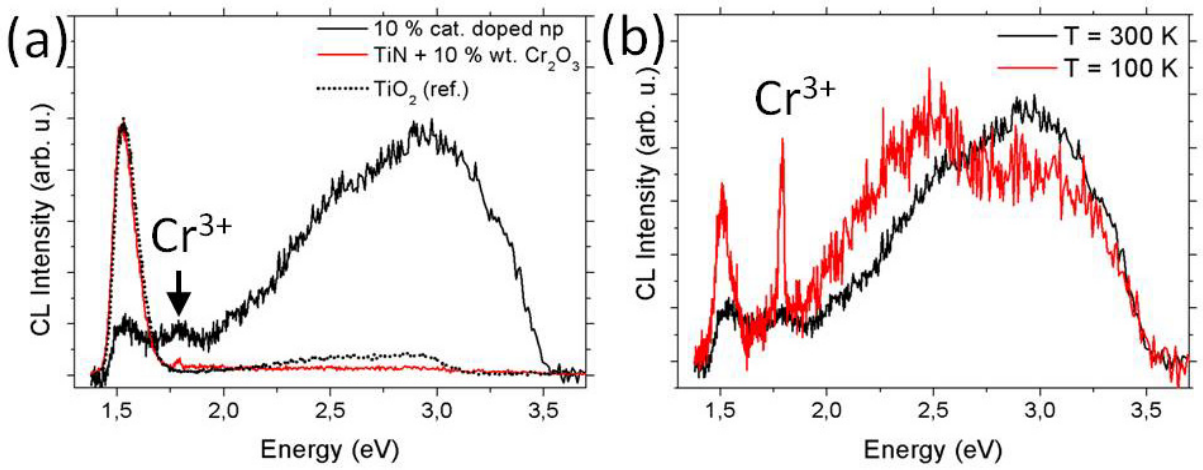

Figure 4. (a) Normalized CL spectra from undoped TiO_2 and microtubes grown using Cr doped TiO_2 nanoparticles (10% cat.) and TiN mixed with Cr_2O_3 (10% wt.). (b) CL spectra from microtubes grown using Cr doped TiO_2 nanoparticles acquired at T = 100 K and T = 300 K.

3.2. Hexagonal ZnO micro and nanotubes

In addition to the rutile SnO_2 and TiO_2, microtubes of hexagonal wurtzite ZnO have been grown by this method. ZnO microtubes were fabricated by a vapor solid process using metallic Zn as precursor and thermal treatments at 700 ºC for 2–4 hours. In that case, the microtubes, with lengths of tens of microns and widths of a few microns (Figure 5a), show hexagonal sections. ZnO presents three fast growth directions along [0001], [10-10], [2-1-10]. Among them the [0001] direction exhibits the maximal growth rate whereas the (2-1-10) are the most stable surfaces [18], which is in agreement with the hexagonal appearance of the ZnO tubes presented here. The ZnO tubes usually appear partially filled, which in some cases results in narrow cavities. CL spectra from the ZnO tubes, shown in Figure 5b, are dominated by an intense emission around 3.2 eV and a broad band with a low relative intensity at 2.4 eV. The former is associated to near bandgap emission, while the green band at 2.4 eV is commonly associated to Zn interstitials and oxygen vacancies defects in ZnO [28]. Most of the works

which report the growth of ZnO tubes are based on hydrothermal or wet chemical methods, usually leading to amorphous or polycrystalline materials. Fewer authors referred the growth of single-crystalline ZnO microtubes [18,29], similar to those analyzed in the present work. In those cases, an oxidation-sublimation process without using catalysts or carrier gases is proposed for the growth of the tubes, which also exhibit hexagonal cross sections. In that process a Zn/Zn suboxide nanostructure is formed at the beginning. The initial nuclei rod reacts continuously with oxygen to form an outer shell ZnO by surface oxidation, acting graphite as reducing agent. The remaining Zn core inside the rods is finally sublimated, due to the high temperature employed in the process which reachs 1000 ºC. In our case, a similar process is proposed, although an argon flow is employed throughout the vapor-solid process leading to the growth of ZnO microtubes, and no reducing agent is needed. Moreover, this vapor-solid process occurs at lower temperatures, avoiding the sublimation of Zn.

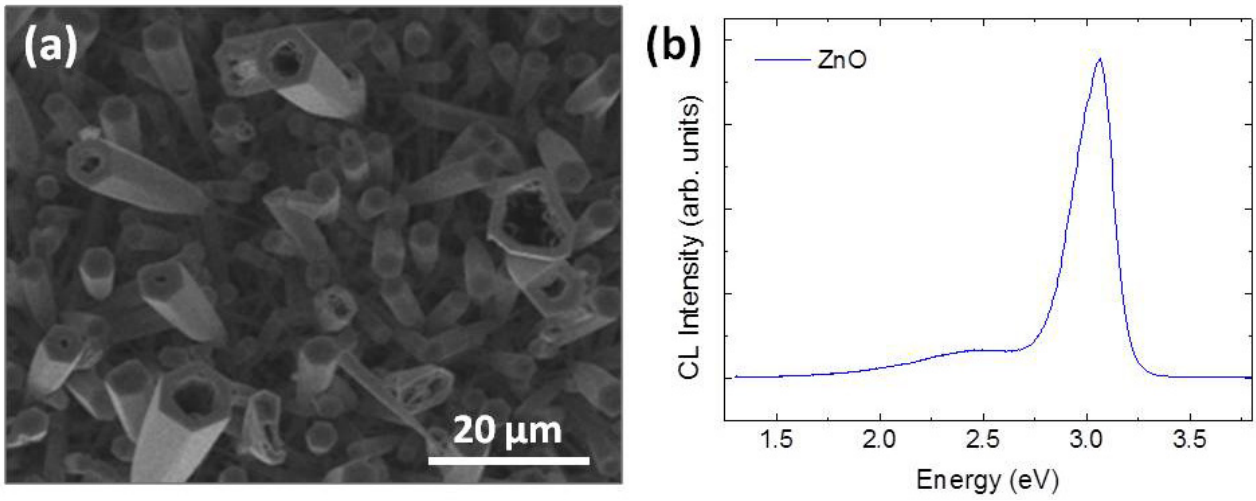

Figure 5. (a) SEM image of a group of ZnO microtubes and (b) the corresponding CL spectrum.

3.3. Hollow elongated structures in cubic materials (In_2O_3 nanopipes)

In this work, either InN or In_2S_3 have been used as precursors to fabricate In_2O_3 elongated micro and nanostructures with a hollow core. When using InN as precursor, tubular micro and nanostructures of bixbyite In_2O_3 were obtained by thermal treatments at 650–750 ºC for 5–10 hours. These treatments lead to the formation of In_2O_3 micro and nanoarrows and rods of tens of microns length and hundreds of nanometers width [30]. TEM measurements demonstrate the presence of a hollow core, named as nanopipe [10], as shown in Figure 6a. These nanopipes, with a width of around 20 nm, independently of the cross section of the structure, extend along the core of the arrows and rods. Vapour-Solid growth has been commonly used as fabrication technique of In_2O_3 elongated structures, however, the driven force behind the VS process for these 1-dimensional cubic In_2O_3 structures is still unclear. Some authors have proposed a supersaturation driven process, where low supersaturation conditions would lead to a 3D growth mode, whereas high supersaturation would induce an anisotropic 1D growth [31]. An autocatalytic process has also been used to explain the 1D growth, arguing that the formation of liquid indium droplets during the growth could support this growth mode as in a Vapor-Liquid-Solid process [32]. In the case of the tubular structures analyzed in the present work, the uniformity in the

inner channel section, independent of the section of the structure, is an evidence of the relaxation mechanism induced by screw dislocations with giant Burgers vectors, as proposed by Frank [33]. Therefore, the presence of the pipes can be associated with a dislocation-driven growth mechanism which governs the formation of the In_2O_3 elongated structures [10]. This method, firstly proposed first by Sears [34] to explain the rapid growth of Hg whiskers, has been recently applied to explain the growth of PbS nanotrees [35] and nanoplates of different materials. The dislocation related steps at the surface are preferential points for the adsorption of new molecules, promoting the growth of 1D structures.

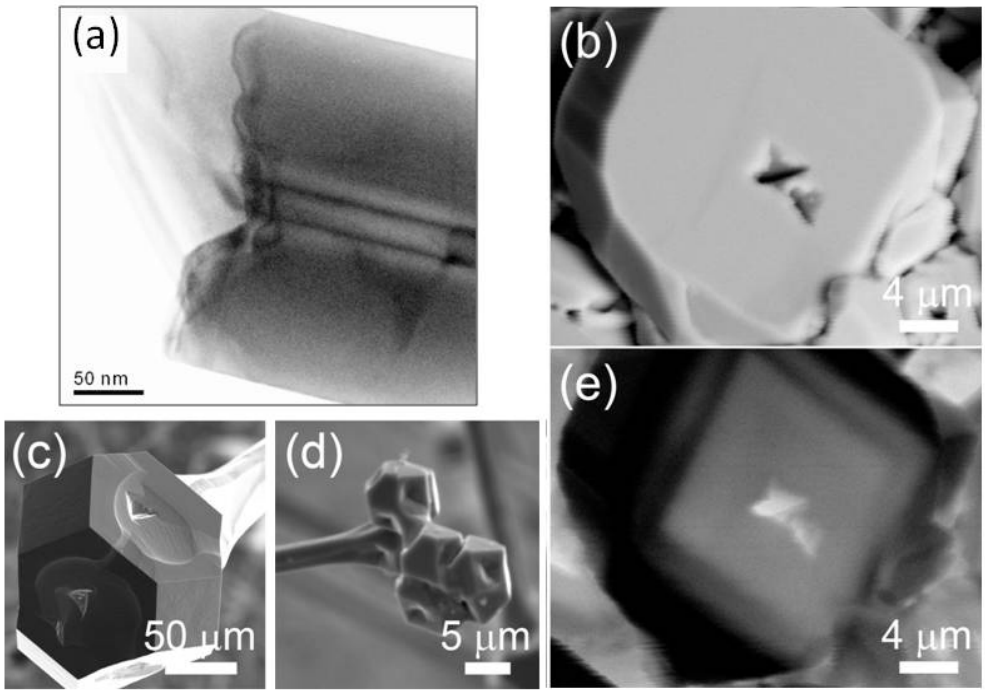

Figure 6. (a) TEM image of a In_2O_3 rod grown from InN with a nanopipe along the core. (b) SEM image of a In_2O_3microcrystal with a pinhole, grown from In_2S_3. (c), (d) SEM images of In_2O_3 cuboctahedral microcrystals grown at the apex of microrods, with facetted pinholes. (e) CL image corresponding to the crystal shown in (b).

Evidences of this mechanism driving the growth of other hollow and compact indium oxide structures have been observed in samples grown using In_2S_3 instead of InN as precursor, and thermal treatments at 950 ºC for 10 hours. Figures 6b–d show respectively the images of a In_2O_3 microcrystal grown at the substrate, and two different microrods with cuboctahedral microcrystals at their apex. Both kinds of microcrystals (either grown at the substrate or at the tip of the rods) are formed by a combination of (111) and (100) surfaces and present facetted pinholes at the centre of their faces. The shape of the pinholes depends on the specific crystalline plane of the microcrystal faces, being triangular for (111) faces, and squared for (100) faces. Pyramidal and octahedral growth of In_2O_3 exhibiting {111} lateral faces has been reported, which correspond to the equilibrium shape of cubic-lattice crystallites determined by a higher growth rate in the [100] direction [36]. Meanwhile cubic shaped indium oxide crystals have been described to grow along the [111] direction exhibiting {100} family plane facets [37,38]. A competition between both processes is produced depending

mainly on the supersaturation and temperature of the growth atmosphere and the growth direction and therefore the shape of the crystals will depend on the ratio between the growth rate along the [100] and [111] directions. Pinholes have been previously associated with the emergence of dislocations at the surface [29,39,40]. CL images obtained from these structures (Figure 6e) show a typical bright and dark contrast usually associated to the presence of dislocations.

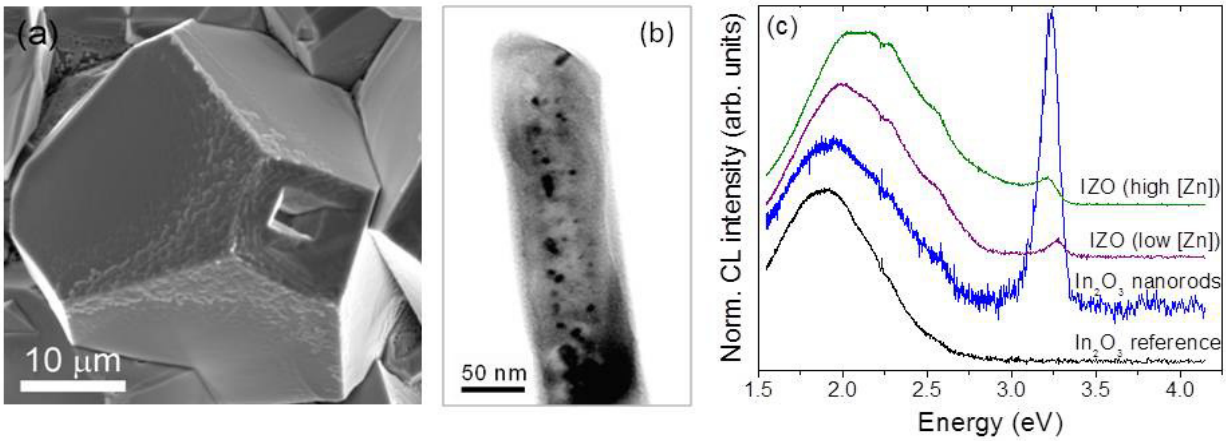

Figure 7. (a) SEM image from a Zn doped In_2O_3 pyramidal microcrystal with a facetted pinhole at the apex. (b) TEM image from a Sn doped In_2O_3 rod, where dark regions corresponding to metallic Sn decorate the central nanopipe. (c) CL spectra acquired in undoped and Zn doped In_2O_3 microstructures.

Doping In_2O_3 with Zn or Sn leads to the formation of, respectively, hollow truncated micropyramids presenting a large pinhole at the surface [41], as it can be observed in Figure 7a, and tubular nanoarrows filled with a core decorated with metallic Sn [42], as shown in Figure 7b, among other structures. Zn-doped In_2O_3 structures were grown using a mixture of InN and ZnO (5% wt.) powders as precursors and thermal treatments at 900 ºC for 10 h, while for Sn-doped In_2O_3 structures a mixture of InN and SnO_2 (10% wt.) was used and thermal treatments at 650 ºC. CL spectra of indium oxide elongated structures (Figure 7c) show a characteristic band centered at around 1.9 eV, which sometimes presents a broadening in the high energy tail at around 2.9 eV. The origin of the high-energy emission band is related to the presence of oxygen vacancies, as established by several works [43,44]. The origin of the 1.9 eV characteristic band, on the other hand, is still unclear. Some authors have attributed it to the presence of oxygen vacancies, however, the results from some works are in clear contradiction to this hypothesis [30,45]. Some other works have related this band to a good crystalline quality [46]. For Zn content below 2% at., Zn-doped indium oxide structures show a luminescence spectrum which is identical to that of undoped indium oxide. However, for a Zn concentration above 2% at., the CL spectra show a broad and complex band peaked at 2.1 eV, with a long tail at the high energy range covering the whole optical range up to the band edge emission at 3.2 eV. The band edge emission, which is not present in the undoped structures, can be resolved as a single peak the energy of which decreases with increasing Zn content [41]. The 2.1 eV band, on the other hand, does not show an energy shift, but its overall intensity increases with Zn content The emissions from the high energy tail increases faster than the 2.1 eV peak. The different behaviours observed for Zn contents below and

above 2% at. have been related to the formation of indium zinc oxide (IZO) ternary compounds with the general chemical formula $In_2Zn_kO_{(k+3)}$.

4. Conclusion

To summarize, different tubular micro- and nanostructures have been fabricated by a vapor-solid method, which avoids the use of templates or catalysts. The growth of SnO_2, TiO_2, ZnO or In_2O_3 elongated hollow structures has been achieved using different precursor powders and thermal treatments. Following this procedure, rutile (SnO_2, Cr doped TiO_2) well-facetted microtubes with rectangular sections are obtained, as well as ZnO microtubes with hexagonal sections and variable diameter of the inner channel. Moreover, In_2O_3 elongated structures showing a hollow core, named as nanopipe, have been fabricated by this method. The morphology and optical properties of these tubes vary when doping with different elements (Cr, Er, Li, Sn, Zn). Dopant contents about 0.5–3% at. have been achieved by this method. CL analysis shows that variations in the luminescence can be associated directly with the dopants (as the 1.79 eV and 0.8 eV emissions related to Cr^{3+} and Er^{3+}, respectively), or to a modification in the defects caused by doping. Different growth mechanisms are proposed for the anisotropic growth leading to the tubes fabricated by the VS process. Despite the fact that diverse mechanisms, such as anisotropic growth, self-catalytic growth, defect-induced growth and oxide assisted growth, have been usually considered to be involved in the VS process, the microscopic nature of the growth mechanisms as well as the driving forces leading to the growth of elongated micro- and nanostructures are not completely understood so far. Parameters such as vapor pressure, supersaturation ratios and surface energies are involved in the VS anisotropic growth, therefore variation of these parameters due to the thermal treatments or the doping process should be considered in the study of the growth of elongated structures by VS. The intrinsic anisotropic character associated with the rutile (SnO_2, TiO_2) and wurtzite (ZnO) lattices can partially explain the growth of elongated structures by the VS process, while for cubic In_2O_3, defects, such as dislocations, should be also involved in the growth of elongated microstructures. Actually, the presence of pipes in the In_2O_3 elongated structures can be explained attending to a dislocation-driven growth mechanism. Moreover the surface energy associated to the different faces forming the tubes should be also considered. The characteristic morphology of these tubular structures, as well as the capability of being filled, can widen their applicability in diverse fields of research, for which a deeper understanding of their properties and growth mechanisms is required. Recent works report on the use of micro- and nanotubes as sensors in environmental applications, optoelectronics, nanosolders and nanothermometers.

Acknowledgments

This work was supported by UCM-Banco Santander, program GR3/14 and MINECO (Project Nos. MAT 2012-31959, MAT 2015-65274-R and Consolider Ingenio CSD 2009-00013).

Conflict of Interest

The authors declare no conflict of interest.

References

1. Iijima S (1991) Helical microtubules of graphitic carbon. *Nature* 354**:** 56–58.
2. Rivaldo-Gómez CM, Cabrera-Pasca GA, Zuniga A, et al. (2015) Hierarchically structured nanowires on and nanosticks in ZnO microtubes. *Sci Rep* 5: 15128.
3. Wang S, He Y, Liu X, et al. (2011) Large scale synthesis of tungsten single crystal microtubes via vapor-deposition process. *J Cryst Growth* 316: 137–144.
4. Eustache E, Tilmant P, Morgenroth L, et al. (2014) Silicon-microtube scaffold decorated with anatase TiO_2 as a negative electrode for a 3D Lithium-Ion Microbattery. *Adv Energy Mater* 4: 1301612.
5. Lang L, Xu Z (2013) Controllable synthesis of porous alpha-Fe_2O_3 microtube and tube in tube by non coaxial electrospinning. *Chem Lett* 42: 750–752.
6. Wen Z, Wang Q, Zhang Q, et al. (2007) In situ growth of mesoporous SnO_2 on multiwalled carbon nanotubes: a novel composite with porous-tube structure as anode for Lithium batteries. *Adv Funct Mater* 17: 2772–2778.
7. Bae C,Yoo H, Kim S, et al. (2008) Template-directed synthesis of oxide nanotubes: fabrication, characterization, and applications. *Chem Mater* 20: 756–767.
8. Maestre D, Cremades A, Piqueras J (2005) Growth and luminescence properties of micro- and nanotubes in sintered tin oxide. *J Appl Phys* 97: 044316.
9. Vásquez C, Peche-Herrero A, Maestre D, et al. (2013) Cr doped titania microtubes and microrods synthesized by a vapor-solid method. *Cryst Eng Comm* 15: 5490–5495.
10. Maestre D, Haeussler D, Cremades, et al. (2011) Nanopipes in In_2O_3 nanorods grown by a thermal treatment. *Cryst Growth Des* 11: 1117–1121.
11. Wu Y, Yang P (2001) Direct observation of vapor-liquid-solid nanowires growth. *J Am Chem Soc* 123: 3165–3166.
12. Ruffino F, Censabella M, Torrisi V, et al. (2014) Size selected growth of unltrathin SiO_2 nanowires on surface and their decoration by Au nanoparticles. *Mater Res Exp* 2: 025003.
13. Yang W, Wan P, Jia MY, et al. (2015) A novel electronic nose based on porous microtubes sensor arrays for the discrimination of VOCs. *Biosens Bioelectron* 64: 547–553.
14. Zhao XY, Liu B, Cao MH. (2015) Engineering microtubular SnO_2 architecture assembled by interconnected nanosheets for high lithium storage capacity. *RSC Advances* 5:30053–30061.
15. Lee HU, Lee SC, Lee YC, et al. (2014) Innovative three-dimensional (3D) eco-TiO_2 photocatalyst for practical environmental and biomedical applications. *Sci Reports* 4: 6740.
16. Dong H, Sun S, Sun L, et al. (2012) Thermodynamic-effect-induced growth, optical modulation and UV lasing of hierarchical ZnO Fabry–Pérot resonators *J Mater Chem* 22: 3069–3074.
17. Ortega Y, Dieker C, Jäger W, et al. (2010) Voids, nanochannels and formation of nanotubes with mobile Sn fillings in Sn doped ZnO nanorods. *Nanotechnology* 21: 222604.
18. Zhan J, Dong H, Sun S, et al. (2015) Surface-energy-driven growth of ZnO hexagonal microtube optical resonators. *Adv Opt Mater* 4: 126–134.
19. Maestre D, Hernandez E, Cremades A, et al. (2012) Synthesis and characterization of small dimensional structures of Er-doped SnO_2 and Erbium-Tin-Oxide. *Cryst Growth Des* 12: 2478–2484.
20. Dai ZR, Pan ZW, Wang ZL, et al. (2001) Ultra-long single crystalline nanoribbons of tin oxide. *Solid State Commun* 118: 351–354.

21. Oliver PM, Watson GM, Kelsey ET, et al. (1997) Atomistic simulation of the surface structure of the TiO_2 polymorphs rutile and anatase. *J Mater Chem* 7: 563–568.
22. Beltran A, Andrés J, Longo E, et al. (2003) Thermodynamic argument about SnO_2 nanoribbon growth. *Appl Phys Lett* 83: 635.
23. Maestre D, Cremades A, Piqueras J (2004) Cathodoluminescence of defects in sintered tin oxide. *J Appl Phys* 95: 3027–3030.
24. Zhou XT, Heigl F, Murphy MW, et al. (2006) Time-resolved x-ray excited optical luminescence from SnO_2 nanoribbons: Direct evidence for the origin of the blue luminescence and the role of surface states. *Appl Phys Lett* 89: 213109.
25. Kar A, Kundu S, Patra A (2011) Surface Defect-Related Luminescence Properties of SnO_2 Nanorods and Nanoparticles. *J Phys Chem C* 115**:** 118–124.
26. Nogales E, García JA, Méndez B, et al. (2007) Red luminescence of Cr in β-Ga_2O_3nanowires. *J Appl Phys* 101: 033517-1–033517-4.
27. Fernández I, Cremades A, Piqueras J (2005) Cathodoluminescence study of defects in deformed (110) and (100) surfaces of TiO_2 single crystals. *Semicond Sci Technol* 20: 239–243.
28. Urbieta A, Fernandez P, Piqueras J (2001) Cathodoluminescence microscopy of hydrothermal and flux grown ZnO single crystals. *J Phys D-Appl Phys* 34: 2945–2949.
29. Dong H, Chen Z, Sun L, et al. (2010) Single-crystalline hexagonal ZnO microtube optical resonators. *J Mater Chem* 20: 5510–551.
30. Magdas DA, Cremades A, Piqueras J (2006) Growth and luminescence of elongated In2O3 micro- and nanostructures in thermally treated InN. *Appl Phys Lett* 88: 113107.
31. Yin W, Cao M, Luo S, et al. (2009) Controllable synthesis of various In_2O_3 submicron nanostructures using chemical vapor deposition. *Cryst Growth Des* 9: 2173–2178.
32. Zeng F, Zhang X, Wang J, et al. (2004) Large scale growth of In_2O_3 nanowires and their optical properties. *Nanotechnology* 15: 596.
33. Frank FC (1951) Capillary equilibria of dislocated crystals. *Acta Crystallogr* 4: 497–501.
34. Sears GW (1955) A growth mechanism for mercury whiskers. *Acta Metall* 3: 361–366.
35. Bierman MJ, Lau YKA, Kvit AV, et al. (2008) Dislocation-driven nanowires growth and Eshelby twist. *Science* 320: 1060–1063.
36. Wang ZL (2000) Transmission electron microscopy of shape controlled nanocrystals and their assemblies. *J Phys Chem B* 104: 1153–1175.
37. Yan Y, Zhou L, Zhang J, et al. (2008) Large scale synthesis of In_2O_3 nanocubes under nondynamic equilibrium model. *Cryst Growth Des* 8: 3285–3289.
38. Tang Q, Zhou W, Zhang W, et al. (2005) Size controllable growth of single crystal $In(OH)_3$ and In_2O_3 nanocubes. *Cryst Growth Des* 5: 147–150.
39. Qian W, Rohrer GS, Skowronski M, et al. (1995) Open core screw dislocations in GaN epilayers observed by scanning forces microscopy and high resolution transmission electron microscopy. *Appl Phys Lett* 67: 2284–2286.
40. Chen Y, Takeuchi T, Amano H, et al. (1998) Pit formation in GaInN quantum wells. *Appl Phys Lett* 72: 710–712.
41. Bartolome J, Maestre D, Cremades A, et al. (2013) Composition-dependent electronic properties of indium-zinc-oxide elongated microstructures. *Acta Materialia* 61: 1932–1943.

42. Maestre D, Haeussler D, Cremades A, et al. (2011) Complex defect structure in the core of Sn-doped In_2O_3 nanorods and its relationship with a dislocation-driven growth mechanism. *J Phys Chem C* 115: 18083–18087.
43. Mazeera M, Zha M, Calestani D, et al. (2007) Low temperature In_2O_3 nanowire luminescence properties as a function of oxidizing thermal treatments. *Nanotechnology* 18: 355707.
44. Wu X, Hong J, Han Z, et al. (2003) Fabrication and photoluminescence characteristics of single crystalline In_2O_3 nanowires. *Chem Phys Lett* 373: 28–32.
45. Kumar M, Singh VN, Singh F, et al. (2008) On the origin of photoluminescence in indium oxide octahedron structures. *Appl Phys Lett* 92:171907.
46. Korotcenkov G, Nazarov M, Zamoryanskaya M, et al. (2007) Cathodoluminescence emission study of nanocrystalline indium oxide films deposited b spray pyrolysis. *Thin Solid Films* 515: 8065–8071.

AIMS Press